Research Article Vol. 34, No. 10 / 18 May 2026 / Optics Express 18471
Optics EXPRESS

Thin-film lithium niobate based microwave photonic filter with up to 110 GHz tuning range

JINGMEI ZHANG,[1] HAOYU WANG,[1] YUANSHENG TAO,[2] ZIHAN TAO,[3,5] YANDONG HE,[1] XINGJUN WANG,[3,4] CHENG WANG,[2] HANKE FENG,[2,6] AND HAOWEN SHU[3,4,7]

[1]School of Integrated circuits, Peking University, Beijing 100871, China
[2]Department of Electrical Engineering State & Key Laboratory of Terahertz and Millimeter Waves, City University of Hong Kong, Kowloon, China
[3]School of Electronics, Peking University,Beijing 100871, China
[4]Frontiers Science Center for Nano-optoelectronics, Peking University, Beijing 100871, China
[5]zihantao@pku.edu.cn
[6]hankefeng2@cityu.edu.hk
[7]haowenshu@pku.edu.cn

Abstract: Integrated microwave photonic filters (MPFs) are essential components for enabling broadband radio frequency signal processing. However, owing to the deficiency of large-bandwidth electro-optic (EO) modulation devices, traditional integrated MPFs based on III-V or silicon photonic platforms face significant challenges in achieving ultra-wideband operation, particularly when extending to the V/E bands and sub-terahertz range. In this paper, we address this limitation and experimentally demonstrated an integrated MPF with ultra-wideband tunability exceeding 110 GHz and high filtering resolution at the sub-GHz level, based on a monolithic thin-film lithium niobate (TFLN) platform. The TFLN MPF chip comprises a large-bandwidth phase modulator and a low-loss microring resonator (MRR) with an intrinsic Q of 2.62×10^6, achieving bandpass filtering responses based on phase-modulation to intensity modulation (PM-IM) conversion mechanism. By precisely controlling the wavelength deviation between the laser carrier and microring resonance, this MPF achieves continuous tuning of the center frequency from near DC to 110 GHz, while maintaining narrow filtering bandwidth (<350 MHz) across the entire tuning range. Compared to state-of-the-art integrated solutions, the proposed TFLN MPF improves the filtering tunable range by nearly two times and extends the operating frequency of MPF beyond 110 GHz for the first time. Our work establishes a foundation for future millimeter-wave and sub-terahertz applications, ranging from 6G ultra-high-speed wireless communication to high-resolution radar.

1. Introduction

Microwave filters are key building blocks in radio-frequency (RF) front-ends, playing a crucial role for signal processing in radar detection, wireless communication, and precision sensing [1–4]. Despite widespread deployment in the sub-6 GHz and centimeter-wave ranges over the past decades, traditional electronic-based filters have encountered significant "electronic bottlenecks" [5–7] that hinder the further expansion of their operating frequency, substantially limiting their applicability in next-generation RF systems. For example, future 6G communication systems are expected to support ultra-high data rates exceeding 100 Gb/s, which requires the exploitation of millimeter-wave and even sub-terahertz spectrum resources for larger bandwidth [8]. This necessitates that RF front-ends have the ability to operate in these high frequency bands. However, the effective operating frequency ranges of existing electronic filters are typically limited to the tens of GHz [9–11], which is far from meeting these new demands.

#593090 https://doi.org/10.1364/OE.593090
Journal © 2026 Received 10 Feb 2026; revised 2 Apr 2026; accepted 8 Apr 2026; published 11 May 2026

Optics EXPRESS

Microwave photonic filter (MPF), which manipulates RF signals in the optical domain [12,13], is considered as a highly promising solution for overcoming the frequency and bandwidth limitations of traditional electronic filters. Driven by its extensive application opportunities, substantial research achievements have been made in the field of MPF over the past few decades, particularly in terms of architectural innovation and reconfigurability [14–18]. More recently, further miniaturization and performance improvements have been achieved by implementing MPFs on integrated photonic platforms [19–25]. Specifically, SOI platforms leverage mature CMOS technology and have significant advantages in large-scale integration, yet their electro-optic (EO) modulation mainly depends on carrier effects, resulting in limitation of overall insertion loss and processing bandwidth. Consequently, achieving both high efficiency and high fidelity in the millimeter-wave band remains challenging [26]. InP platforms can achieve monolithic integration of active and passive devices to realize a fully integrated MPF [27]. However, their large waveguide propagation loss restrains the quality factor of the resonant structure, thereby restricting the frequency resolution and selectivity of the filter. While silicon nitride (Si_3N_4) platforms can construct high-Q passive optical filters due to their extremely low propagation loss [28], the absence of intrinsic EO effects makes it difficult to achieve high-speed modulation on a single chip, which can lead to increased system complexity and packaging difficulties.

In recent years, the emergence of thin-film lithium niobate (TFLN) provides a compelling platform to address these trade-offs between filtering performance and system integration level [29]. Specifically, TFLN platform offers strong Pockels effect to achieve ultra-high bandwidth (>110 GHz) [30] and low-drive-voltage (below 1 V) [31] linear modulation, which enables the RF signals across a broad frequency range to be broadcasted onto optical domain with high linearity and excellent signal fidelity. Additionally, advances in fabrication processes have enabled the realization of high-Q microring resonators (MRRs) with intrinsic Q up to 2.93×10^7 [32], corresponding to an ultra-low propagation loss of 1.3 dB/m. The optical filtering responses of such high-Q MRRs can directly translate into narrow RF filter passbands—at the sub-GHz, or even sub-MHz, level—thereby providing a key device foundation for fine spectral control in the optical domain. In short, the critical ability to co-integrate high-performance EO modulation and ultra-low-loss passive photonic devices on a single chip positions TFLN a strong candidate for microwave photonic systems that demand both wide bandwidth and high processing fitness.

Despite the promise of TFLN platform for integrated MPFs [33], existing demonstrations have not yet monolithically incorporated both large-bandwidth EO modulation and high-Q optical filtering devices on a single chip, which would fully exploit the technical advantages of the platform [34]. To date, state-of-the-art integrated MPFs on TFLN platform typically operate up to 62 GHz and exhibit a filtering resolution of approximately 0.7-3 GHz [35], which still does not fully unlock the performance potential of TFLN for ultra-wideband and high-resolution filtering. Moreover, systematic investigations of long-term operation stability and end-to-end RF link performances remain relatively scarce. Here, we demonstrated a high-performance integrated MPF based on the TFLN platform featuring record-wide operating frequency range. By integrating an ultrawideband phase modulator (PM) and a high-Q MRR onto a single chip, this integrated MPF achieves a continuously tunable bandpass filtering response over an ultrawide frequency range of 0–110 GHz. Notably, thanks to the ultralow propagation loss of the TFLN waveguide, the filter exhibits excellent spectral selectivity, maintaining a stable 3 dB filtering bandwidth of 227–331 MHz throughout the entire tuning range, while the total filter loss is as low as 26.1–28.3 dB. Furthermore, the linearity of the system was evaluated using two-tone measurements, yielding a spurious-free dynamic range (SFDR) of 74.4–83.74 $dB \cdot Hz^{2/3}$. A one-hour stability measurement was also conducted, revealing reliable steady-state performance without the need for active feedback control, which highlights the robustness and practicality of the proposed integrated MPF. Compared to existing integrated solutions, its effective tuning range is improved by nearly two times, opening up what we believe is a new technological path

Optics EXPRESS

for next-generation high-performance, reconfigurable millimeter-wave and sub-terahertz signal processing chips.

2. Operation principles

Figure 1 shows the system architecture of the proposed monolithically integrated tunable MPF based on TFLN platform. The TFLN-based MPF mainly consists of a continuous-wave (CW) laser, a PM, an MRR, and a high-speed photodetector (PD). The core working principles of the system is based on the mapping conversion effect from phase-modulation to intensity modulation (PM-IM) [36]. The RF signal to be processed at a frequency of ω_{rf} first drives the TFLN high-speed PM, loading the modulation information onto a coherent optical carrier with an angular frequency of ω_c. Under small signal modulation conditions, the modulated spectrum consists of symmetrically distributed positive and negative first-order sidebands with equal amplitude and opposite phase, with angular frequencies of $\omega_{c-}\omega_{rf}$ and $\omega_{c+}\omega_{rf}$. Due to this symmetry, a significant destructive interference occurs when the modulated optical signal is directly photodetected without spectral shaping. This results in a strong spectral suppression in the RF domain, providing an extremely low background noise for subsequent filtering. To achieve narrow bandpass filtering, the modulation light is injected into the high-Q MRR monolithically integrated with the phase modulator. The MRR selectively alter the amplitude and phase of a modulation sideband through their narrow linewidth resonance characteristics, thereby disrupting the original symmetrical sideband cancellation. When a resonance peak is precisely aligned with the modulation sideband, the output spectrum exhibits significant asymmetry. Upon coherent photo-detection in a high-speed PD, the condition for destructive interference is broken, allowing the RF signal to be recovered. As a result, a narrow bandpass response is reconstructed in the RF domain, exhibiting a one-to-one correspondence with the optical resonance profile. By controlling the relative detuning between the optical carrier and the microring resonant peak, the system can achieve continuously tunable bandpass filtering in the RF domain, thereby completing the mapping process from optical spectral shaping to RF filtering, as shown in Fig. 1.

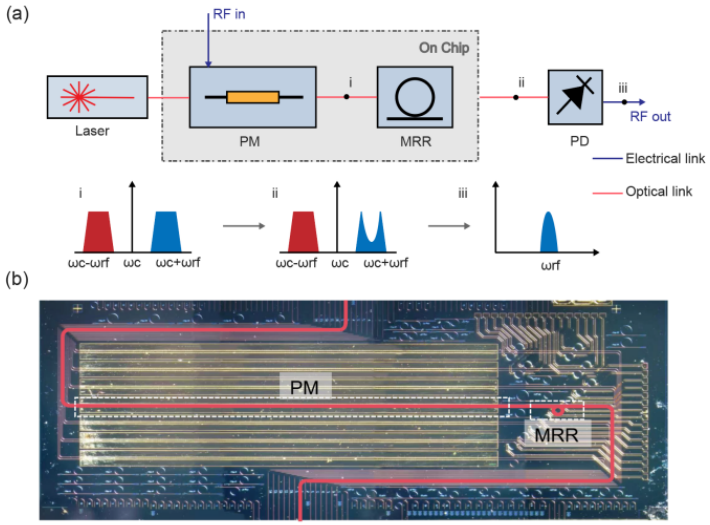

Fig. 1. (a) The operation principles for the bandpass filtering response of the integrated MPF. (b) Top-view micrograph of the TFLN chip. Noted that the highlighted optical propagation path of PM and MRR is roughly showed, due to their relatively small size.

Optics EXPRESS

3. Experimental results

3.1. Chip design and fabrication

The detailed fabrication flow is depicted in Fig. 2. Devices are fabricated with a SiO_2 layer serving as an etching hard mask on a 4-inch LNOI wafer, using plasma-enhanced chemical vapor deposition (PECVD). Subsequently, an ASML UV stepper lithography system (NFF, HKUST) is used to expose each 1.5 cm × 1.5 cm chip cell at approximately 500 nm resolution, forming optical waveguides, PM, and MRR across the entire wafer. During etching, a photoresist pattern is first transferred to the SiO_2 hard mask layer using fluorine-based dry etching. Then, an optimized Ar^+ -based inductively coupled plasma (ICP) reactive-ion etching process is used to precisely etch the pattern to the LN device layer, resulting in a film approximately 250 nm thick. After etching, the residual SiO_2 mask is removed, a protective layer is redeposited, and annealing is performed to improve optical performance. Subsequently, the microwave electrodes, on-chip heaters, and wires/pads, were fabricated using second, third, and fourth photolithography and lift-off processes, respectively.

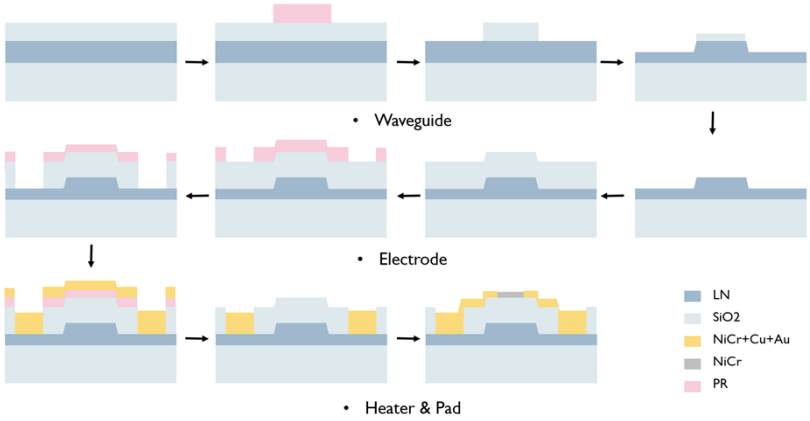

Fig. 2. Process flow on TFLN wafer

Regarding device structure, the phase modulator employs a slotted traveling-wave electrode design to enhance EO bandwidth. The electrode length is approximately 10 mm. The MRR is based on a 250 nm ridge waveguide and designed as an all-pass structure with a FSR of approximately 222 GHz. The waveguide width is set to 1.2 µm, and the bending radius is 94 µm. The resonance wavelength of the MRR can be tuned using a NiCr microheater. The chip has an effective size of approximately 7.6 mm × 15 mm. The TFLN photonic chip incorporates high-performance PM and high-Q MRR on a same platform, providing a solid foundation for broadband, low-loss, and high-stability millimeter-wave photonic filters.

3.2. Characterization of key devices

The filtering bandwidth of the proposed integrated MPF is mainly limited by the optical characteristics of the on-chip passive filtering component. Figure 3(a) shows a typical transmission spectrum of the TFLN MRR. Lorentzian fit analysis revealed a full width at half maximum (FWHM) of 1.9 pm, which corresponds to a load quality factor (Q_L) of 8.26×10^5. Further calculations based on the fitting results indicate that the intrinsic Q value (Q_i) of this device reaches 2.62×10^6. This low loss characteristic allows the integrated MPF to achieve a narrow optical filtering linewidth down to sub-GHz level, resulting in high frequency selectivity in the millimeter-wave band. Given that the PM-IM conversion mechanism of the MPF is highly dependent on the breaking of spectral symmetry, we characterized the phase response of the

Optics EXPRESS

MRR using high-resolution optical vector analysis (OVA), as shown in Fig. 3(b). Experimental results revealed a phase abrupt change of nearly 180° at the resonant frequency, indicating that the microring is in over-coupled state. This dramatic phase evolution is crucial for eliminating destructive interference between PM upper/lower sidebands for constructing bandpass filtering response upon photo-detection. Furthermore, the tunability of the MPF central frequency is achieved through a NiCr microheater integrated above the waveguide. As shown in Fig. 3(c), by increasing the driving voltage from 0 V to 22 V, the resonant wavelength of the MRR exhibits a stable continuous redshift, with a maximum tuning amount of 0.62 nm. As shown in Fig. 3(d), the thermal power dissipated across the microheater as the drive voltage increases from 0 V to 22 V, with a maximum value of 436.7 mW. This thermo-optic tuning performance, combined with the tunability of the laser wavelength, endows the integrated MPF with ultra-wideband spectral processing capabilities covering the DC to V/E bands. In addition, high-performance EO PMs are core components for realizing MPFs. We characterized the on-chip integrated PM. The insertion loss of the phase modulator is approximately 2.95 dB. Due to the complexity of direct measurement of phase modulators, we derived the frequency response characteristics of the phase modulator by testing an intensity modulator (IM) fabricated under the same process and with the same electrode length. Measurement result shows an around 1.2 dB S_{21} degradation below 67 GHz, with the 3 dB EO bandwidth of this PM exceeded 110 GHz, demonstrating the excellent high-speed response potential of the TFLN platform. Using the Mach-Zehnder interferometry (MZI) assisted testing method assembled by external fibers, its half-wave voltage (V_π) in the DC state was measured to be approximately 4.28-6.2 V.

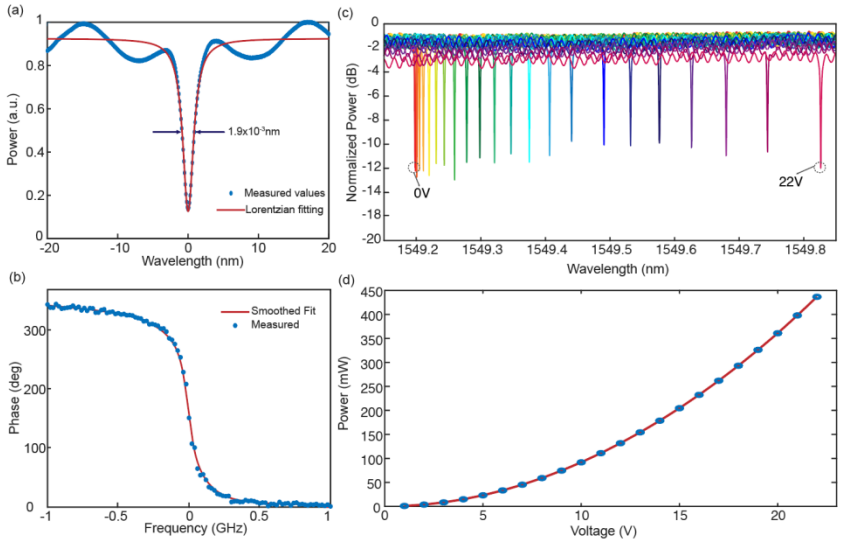

Fig. 3. (a) Measured transmission spectrum of the MRR. (b) Measured phase response within a resonance of the MRR. (c) Measured optical spectra with various DC voltages applied to the microheater. (d) Measured the thermal power dissipated across the microheater with various DC voltages applied to the microheater.

3.3. *RF filtering response*

To quantitatively evaluate the filtering characteristics of this integrated TFLN-MPF, we constructed a measurement setup based on a vector network analyzer (VNA), as shown in Fig. 4. In the experiment, the optical carrier generated by the laser source is coupled into the TFLN chip via an edge coupler. The frequency-swept signal generated by the VNA is applied to the

Optics EXPRESS

on-chip phase modulator through a high-speed microwave probe (T-Plus 110 GHz). The optical modulated signals then undergo spectral shaping by a high-Q MRR, and are finally recovered to the RF domain by an ultra-high bandwidth PD (COHERENT XPDV4120R). By acquiring the S_{21}-transmission response profiles through the VNA, key performance metrics of the integrated MPF such as the center frequency, bandwidth, and rejection ratio can be obtained.

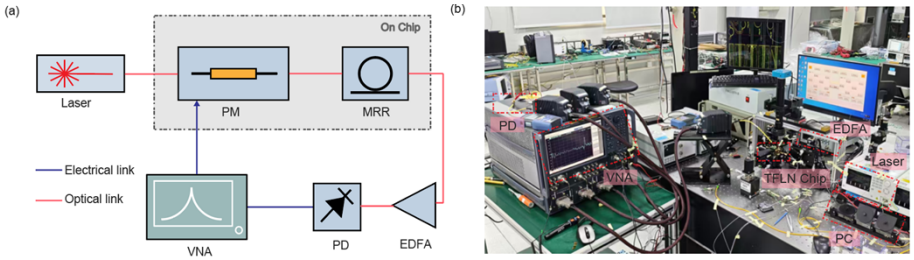

Fig. 4. (a) Experimental setup to measure the filtering response of the integrated MPF. (b) Photograph of the experimental setup.

As shown in Fig. 5(a), the central frequency of the filtering passband can be continuously tuned over the frequency range of near DC to 110 GHz. Here, the maximum high-frequency tuning limit is set by the half-FSR of the MRR to prevent frequency aliasing introduced by its spectral periodicity. Thanks to the ultra-large FSR design of the MRR, which reaches to 222 GHz, the system successfully covers the DC-110 GHz operation frequency band. The linewidth and insertion loss performances of the filter exhibit only minor variations across the entire frequency tuning range, as shown in Fig. 5(b). The measured 3 dB filtering bandwidth varies between 227 MHz and 331 MHz, confirming the excellent gain flatness and consistent filtering resolution of the TFLN MPF. To accurately characterize the ultra-wideband filtering response and compensate the link loss, a driver was employed after the PD to boost the output signal power. This ensured a high signal-to-noise ratio (SNR) across the entire 110 GHz range. The insertion loss of the MPF is within 26.1-28.3 dB, which could be further reduced by mitigating the coupling loss (currently ~10 dB) to increase the input power to the high-speed PD. To clarify the optimization path, we conducted a detailed budget analysis of the link loss. At the optical link level, the loss mainly stems from unoptimized fiber-chip edge coupling (approximately 10 dB/facet). At the chip level, the waveguide propagation loss coefficient is 0.15 dB/cm; for the total waveguide length of 3.47 cm in this device, the in-chip propagation loss is approximately 0.52 dB. The insertion loss of the phase modulator is approximately 2.95 dB, and the insertion loss of the MRR is approximately 0.96 dB. By introducing advanced edge coupling techniques, such as a bident edge coupler [37], a triple layers inverse-tapered structure [38] or a wedgewaveguide edge coupler [39], the coupling loss is expected to be reduced to below 1.5 dB/facet. The above quantitative analysis demonstrates that by addressing the coupling loss, this TFLN platform has significant application potential in realizing high-performance, transparent microwave photonic links.

3.4. *Spurious-free dynamic range*

SFDR is a key performance metrics for evaluating the ability of MPFs to process weak signals under linearity and noise constraints [40]. To quantitatively characterize the SFDR of the integrated TFLN-MPF, we conducted a standard two-tone test, as shown in Fig. 6(a). Due to the operating frequency limitations of the microwave signal generator (MSG) and electronic spectrum analyzer (ESA), five typical frequency points with center frequencies of 1, 5, 10, 15, and 20 GHz were selected for the experiment, in which a dual-channel RF source is utilized to generate two-tone signals with a frequency spacing of 0.1 GHz, which were then applied to the on-chip PM. By precisely adjusting the laser wavelength, it was ensured that the two-tone

Optics EXPRESS

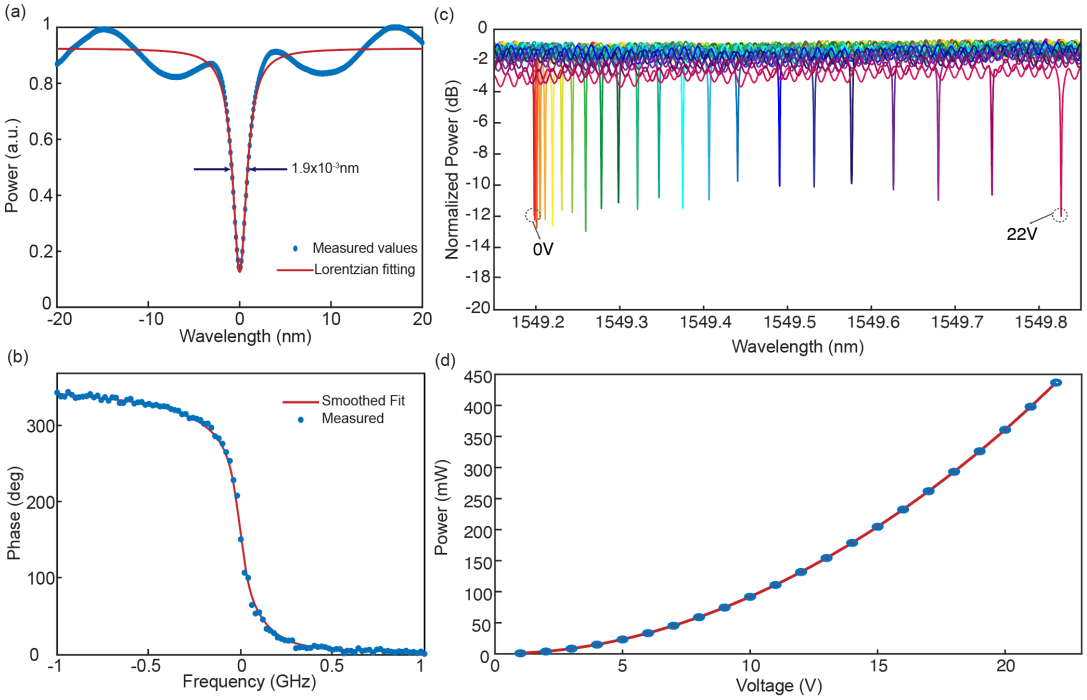

Fig. 5. (a) Measured RF response of the integrated MPF at different center frequencies in the 0-110 GHz range. (b) The variation of 3 dB bandwidth and filter response loss with various RF operation frequency.

components under test were all within the bandpass region of the MPF response. The signal output from the off-chip photodetector was collected and analyzed using an electronic spectrum analyzer (ESA). As the input RF power was incrementally increased, we precisely tracked the power variations of the fundamental (FUND) component and the third-order intermodulation distortion component (IMD3). Figures 6(b)-(f) show the power mapping curves at different measured frequencies. The experimentally measured output noise floor of the system is −150 dBm/Hz. Using the third-order intercept extrapolation method, the third-order intermodulation spurious-free dynamic range ($SFDR_{IMD3}$) at each frequency was calculated, as shown in Fig. 6(g). The measured values located in a range of 74.4 to 83.74 $dB \cdot Hz^{2/3}$. Analysis indicates that as the operating frequency increases, the impact of the notch response of the MRR on the optical carrier decreases, effectively reducing the filter's loss. Benefiting from the extremely stable EO coefficient of the TFLN platform, we expect the system's SFDR performance to remain robust and consistent across the entire ultra-wide tuning range of 110 GHz. The relatively low SFDR obtained in the current experiment is mainly due to the large insertion loss caused by unoptimized fiber-to-chip coupling. The SFDR of a photonic link is highly sensitive to both the RF power gain and the noise floor. Employing advanced edge-coupling technologies to reduce the coupling loss to below 1.5 dB/facet is expected to further improve the SFDR. By maintaining a constant output optical power from the EDFA, a 17 dB reduction in optical loss will effectively lower the amplified noise floor generated by the EDFA by approximately 17 dB. Consequently, although the RF gain of the link remains invariant, the SFDR will be enhanced by approximately 11.3 dB. Beyond coupling optimization, further SFDR breakthroughs can be achieved through optical-domain linearization architectures, such as dual-polarization control [41], and microring-assisted [42,43] or series/parallel MZI configurations [44,45].

Optics EXPRESS

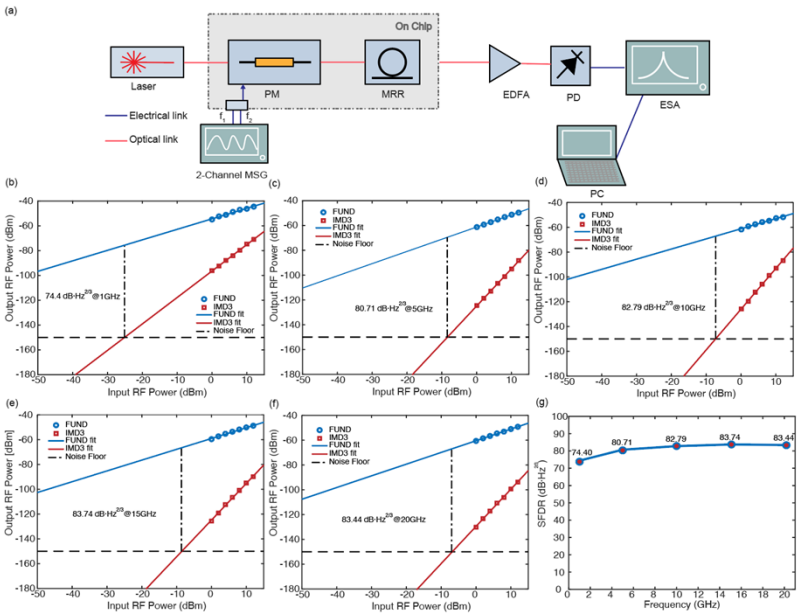

Fig. 6. (a) Experimental setup to measure the SFDR of the integrated MPF. (b)- (f) Measured power of the FUND component and the IMD3 component versus different input RF power. (g) Measured SFDR values under different RF frequency.

3.5. *Long-term stability of the filtering performances*

To evaluate the reliability of the integrated MPF in practical applications, we also quantitatively characterized the long-term stability of its bandpass filtering performances. In the experiment, a thermoelectric cooler (TEC) was used to maintain the operating temperature of the TFLN chip at 23°C (the thermal sensitivity coefficient is −2.3097 GHz/°C), without the need for complex high-speed optoelectronic closed-loop feedback control. We selected three typical frequency points —nearby 1 GHz, 50 GHz, and 107 GHz— and used a VNA to record the RF filter response by repeating sampling five times every 10 minutes over a continuous 1-hour operating cycle. The measurement results are shown in Fig. 7. The experimental results show that the filter maintained high operation stability over the whole monitoring period. Specifically, the filter insertion loss remained stable between 26.3 dB and 28.6 dB at each frequency point, and the 3 dB bandwidth also exhibits consistent values within 0.25 GHz to 0.33 GHz, and the center frequency remained stable between 33 and 100 MHz. These measurement results credibly verifies that the monolithically integrated TFLN-MPF maintain good steady-state operational functionalities even in the absence of active optoelectronic closed-loop feedback control. But subtle performance fluctuations were observed during the long-term monitoring. Specifically, the slight instability in the peak S_{21} is primarily attributed to mechanical perturbations in the fiber-to-chip edge-coupling setup caused by environmental vibrations. Despite the implementation of a TEC to maintain the operating temperature at a stable 23°C, minor drifts in the center frequency and 3 dB bandwidth persist. These are mainly rooted in the imperfect thermal control within the MRR. Residual thermal fluctuations at the micro-scale can still induce minute changes in the refractive index of the waveguide, leading to the observed stochastic jitter in the optical spectra. For applications with higher requirements for performance stability, introducing a more precise closed-loop temperature control system or an on-chip active optoelectronic closed-loop feedback compensation loop will be an effective way to further optimize system robustness and eliminate environmental noise interference.

Optics EXPRESS

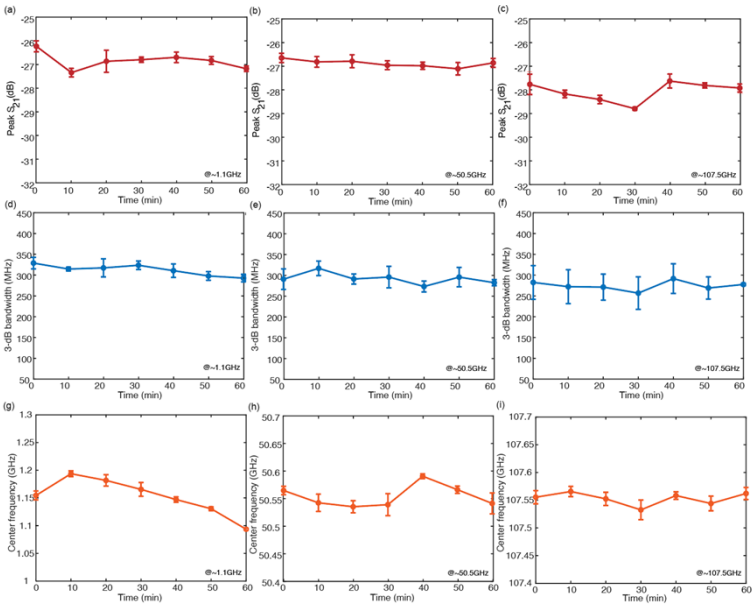

Fig. 7. (a)-(c) Measured insertion loss of the TFLN integrated MPF over 1 h continuous operation at different RF frequencies. (d) - (f) Measured 3 dB filtering bandwidth over 1 h continuous operation at different RF frequencies. (g) - (i) Measured center filtering frequency over 1 h continuous operation at different RF frequencies.

3.6. *Performance comparison and discussion*

To evaluate the overall performance of our proposed integrated MPFs, Table 1 compares its key performance indicators with those of representative state-of-the-art MPFs based on Si_3N_4, SOI, and InP platforms.

Table 1. Summary of the Representative Ultra-Wideband MPFs

Platform	Integrated devices	Q value	Filter type	3 dB Bandwidth	Microring FSR	Tuning Range	SFDR
Si_3N_4 [28]	MRR	$Q_L: 4.36\times10^5$	P	0.61 GHz	1.21 nm	8–38 GHz	/
Si_3N_4 [46]	MRR	$Q_L: 1.7\times10^6$	P	0.36 GHz	1 nm	10–20 GHz	/
SOI [47]	PM + 4MRRs + PD	$Q_L: 1.3\times10^6$	P	0.22 GHz.	0.644 nm	6.1–35.9 GHz	102.1 dB $Hz^{2/3}$@11.15GHz
InP + SOI [17]	PM + MRR	$Q_i: 1.63\times10^6$	P / S	0.30–0.47 GHz/ 0.38–0.45 GHz	0.24 nm	3–21 GHz/ 3–25 GHz	99.7 dB $Hz^{2/3}$@3GHz
InP [28]	RAMZI	/	LP	2.5–5.5 GHz	~ 0.16 nm	0–6 GHz	81.4 dB $Hz^{2/3}$@1.4GHz
InP [48]	SOAs + PMs	/	P	1.9–5.4 GHz	~ 0.188 / 0.376 nm	0–27 GHz	86.3 dB $Hz^{2/3}$@5.9GHz
TFLN [35]	MRR	$Q_L: 2.2\times10^5$	P	0.7-3 GHz.	1nm	2–62 GHz	101.16 dB $Hz^{2/3}$@17.8GHz
TFLN (This Work)	PM + MRR	$Q_i: 2.62\times10^6$	P	0.227–0.331 GHz	1.78nm	0–110 GHz	74.4-83.74 dB/$Hz^{2/3}$@1-20GHz

SOAs:semiconductor optical amplifiers; P:Bandpass; S:Band-stop; LP:Low-pass

Optics EXPRESS

The comparison clearly shows that our demonstrated integrated MPF holds significant advantages in key performance metrics—including frequency coverage, filtering resolution, and broadband stability—over existing approaches. The device simultaneously achieves an ultra-wide continuous tuning range (0–110 GHz) and fine frequency selectivity (3 dB bandwidth of 227–331 MHz). More importantly, these high filtering performances are consistently maintained across the entire frequency band with only minor variations. This capability is critically valuable for next-generation RF front-ends, which are expected to operate across multi-band frequency ranges from microwave to sub-terahertz regimes. While the Si_3N_4 platform could achieve ultra-high Q factor and sub-GHz narrowband filtering due to extremely low propagation loss, the large bending radius required to maintain low loss significantly limits the device's FSR, typically restricting its operating frequency to meet the needs of broadband microwave and millimeter-wave applications. The InP platform possesses the unique advantage of monolithic integration of all desired active devices, but its high waveguide propagation loss (approximately 5.5 dB cm^{-1}) severely restricts the Q value of the resonant cavity, resulting in a poor filtering resolution. Regarding the SOI platform, while it benefits from mature CMOS-compatible processes and enable large-scale integration, its modulator bandwidth is fundamentally limited by free-carrier dispersion effects, typically below 40 GHz, and it also suffer from severe nonlinear distortion for large analog signal input.

In contrast, the TFLN integrated platform used in this work fully leverages its advantages, including Pockels EO coefficient of $r_{33} = 30.8$ pm/V, low optical loss of 0.15 dB/cm, and intrinsic high linearity. First, the pure EO mechanism of TFLN materials avoids carrier effects, fundamentally ensuring high linear response over ultra-wideband frequency range. Second, the low-loss waveguide combined with an optimized resonant cavity design ensures that the device maintains fine linewidths at sub-GHz level. More importantly, through the synergistic optimization of traveling-wave electrodes and a large FSR microring architecture, we extended the frequency tuning range to 110 GHz while maintaining stable filtering performance over a wide bandwidth. Specifically, the traveling-wave electrode has a slotted electrode size of 10 mm, a slot length of 5 μm, a slot width of 2 μm, and a GS electrode spacing of 5 μm. To our knowledge, this represents the widest continuously tunable microwave filtering range reported in integrated photonic platforms.

4. Summary

In summary, we have experimentally demonstrated an ultrawideband, frequency-agile integrated MPF based on a monolithic TFLN platform, addressing the bandwidth limitations and tunability bottlenecks of traditional electronic filters in the millimeter-wave band. Experimental results show that this integrated MPF achieves continuous, unambiguous tuning of the center frequency from near DC to 110 GHz, covering a broad spectrum from low-frequency microwaves to high-frequency millimeter waves. Thanks to the ultra-low propagation loss of the TFLN waveguide, the filter exhibits excellent selectivity, with a bandpass filtering bandwidth of 227–331 MHz. Two-tone testing confirmed the good linearity of this integrated MPF, with its $SFDR_{IMD3}$ remaining stable between 74.4–83.74 dB/$Hz^{2/3}$. Furthermore, a one-hour stability test demonstrated the system's reliable steady-state performance without the need for active feedback control. This work provides an efficient on-chip solution for ultra-wideband millimeter-wave communication and high-resolution radar, and also demonstrates promising potential for the design and implementation of other integrated microwave photonic functional systems that simultaneously requires large-bandwidth and high processing resolution.

Funding. National Natural Science Foundation of China under grants (62322501, 62235002, 62327811); Fundamental and Interdisciplinary Disciplines Breakthrough Plan of the Ministry of Education of China(JYB2025XDXM121); Research Grants Council, University Grants Committee (STG3/E-704/23-N, JRFS2526-1S01); Fundamental and Interdisciplinary

Optics EXPRESS

Disciplines Breakthrough Plan of the Ministry of Education of China, and Guangdong and Hong Kong Universities '1+1+1' Joint Research Collaboration Scheme.

Acknowledgment. This work was supported by High-performance Computing Platform of Peking University.

Disclosures. The authors declare no conflicts of interest.

Data availability. Data underlying the results presented in this paper are not publicly available at this time but may be obtained from the authors upon reasonable request.

References

1. J. Yao, "Microwave photonics," J. Lightwave Technol. **27**(3), 314–335 (2009).
2. J. Capmany and D. Novak, "Microwave photonics combines two worlds," Nat. Photonics **1**(6), 319–330 (2007).
3. C. Liu, J. Wang, L. Cheng, *et al.*, "Key microwave photonics technologies for next-generation cloud-based radio access networks," J. Lightwave Technol. **32**(20), 3452–3460 (2014).
4. J. Hervás, A. L. Ricchiuti, W. Li, *et al.*, "Microwave photonics for optical sensors," IEEE J. Sel. Top. Quantum Electron. **23**(2), 327–339 (2017).
5. F. Camponeschi, M. Reza, C. Porzi, *et al.*, "Integrated microwave photonic receiver for radar applications," *24th European Conference on Integrated Optics* (2023).
6. W. Saad, M. Bennis, and M. Chen, "A vision of 6 g wireless systems: Applications, trends, technologies, and open research problems," IEEE Netw. **34**(3), 134–142 (2020).
7. Y. Liu, A. Choudhary, D. Marpaung, *et al.*, "Integrated microwave photonic filters," Adv. Opt. Photonics **12**(2), 485–555 (2020).
8. Z. Tao, H. Wang, H. Feng, *et al.*, "Ultrabroadband on-chip photonics for full-spectrum wireless communications," Nature **645**(8079), 80–87 (2025).
9. A. Boutejdar, A. A. Ibrahim, and W. A. E. Ali, "Design of compact size and tunable band pass filter for WLAN applications," Electron. Lett. **52**(24), 1996–1997 (2016).
10. E. J. Naglich, A. C. Guyette, and D. Peroulis, "High-Q intrinsically-switched quasi-absorptive tunable bandstop filter with electrically-short resonators," *2014 IEEE MTT-S International Microwave Symposium (IMS2014)*, pp. 1–4.
11. S. Courreges, Y. Li, Z. Zhao, *et al.*, "A Ka-band electronically tunable ferroelectric filter," IEEE Microw. Wireless Compon. Lett. **19**(6), 356–358 (2009).
12. X. Zou, B. Lu, W. Pan, *et al.*, "Photonics for microwave measurements," Laser Photonics Rev. **10**(5), 711–734 (2016).
13. S. Pan and J. Yao, "Photonics-based broadband microwave measurement," J. Lightwave Technol. **35**(16), 3498–3513 (2017).
14. Y. I. A. Al-Yasir, N. Ojaroudi Parchin, R. A. Abd-Alhameed, *et al.*, "Recent progress in the design of 4 g/5 g reconfigurable filters," Electronics **8**(1), 114 (2019).
15. R. Levy and S. B. Cohn, "A history of microwave filter research, design, and development," IEEE Trans. Microw. Theory Tech. **32**(9), 1055–1067 (1984).
16. Z. Tao, Y. Tao, M. Jin, *et al.*, "Highly reconfigurable silicon integrated microwave photonic filter towards next-generation wireless communication," Photonics Res. **11**(5), 682–694 (2023).
17. Y. Tao, H. Shu, X. Wang, *et al.*, "Hybrid-integrated high-performance microwave photonic filter with switchable response," Photonics Res. **9**(8), 1569–1580 (2021).
18. Z. Tao, B. Shen, W. Li, *et al.*, "Versatile photonic molecule switch in multimode microresonators," Light: Sci. Appl. **13**(1), 51 (2024).
19. C. Wei, H. Feng, K. Ye, *et al.*, "Programmable multifunctional integrated microwave photonic circuit on thin-film lithium niobate," Nat. Commun. **16**(1), 2281 (2025).
20. Y. Shi, Y. Yu, Y. Liu, *et al.*, "Intelligent Configuration of Integrated Microwave Photonic Filter Featuring Self-Stabilization and Programmable Response," Laser Photonics Rev. **20**(4), e01962 (2026).
21. Y. Tao, H. Feng, Y. Fang, *et al.*, "Integrated photonic ultrawideband real-time spectrum sensing for 6G wireless networks," Nat. Commun. (2026).
22. H. Shu, B. Shen, H. Chang, *et al.*, "Microcomb technology: from principles to applications," Photonics Insights **3**(4), R09 (2024).
23. W. Zhang, Z. Li, Z. Wang, *et al.*, "Wideband-tunable programmable microwave photonic filter on silicon," *OptoElectronics and Communications Conference and Photonics in Switching and Computing* 1–3 (2025).
24. Z. He, Z. Wang, H. Yan, *et al.*, "Photonics-assisted microwave frequency measurement based on high-Q micro-ring resonator," Proc. SPIE **13648**, 136480C (2025).
25. Z. Chen, H. Wang, A. Zhang, *et al.*, "Ultra-high sensitivity integrated photonic biosensors based on a feedback-coupled microring resonator," Opt. Express **33**(5), 10355–10363 (2025).
26. W. Zhang and J. Yao, "Silicon-based integrated microwave photonics," IEEE J. Quantum Electron. **52**(1), 0600412 (2016).
27. J. S. Fandiño, P. Muñoz, D. Doménech, *et al.*, "A monolithic integrated photonic microwave filter," Nat. Photonics **11**(2), 124–129 (2017).
28. T. Cui, D. Liu, F. Liu, *et al.*, "Tunable optoelectronic oscillator based on a high-Q microring resonator," Opt. Commun. **536**, 129299 (2023).

Optics EXPRESS

29. Y. Zhang, H. Shu, Y. Guo, *et al.*, "Integrated photonics enabling ultra-wideband fibre–wireless communication," Nature **651**(8105), 348–355 (2026).
30. Y. Liu, Z. Zhou, P. Zhou, *et al.*, "Volume manufacturing of thin-film lithium niobate modulators with bandwidth > 110 GHz based on 4-inch wafer with a quartz handle," Light: Adv. Manuf. **14**(1), 47 (2025).
31. G. Chen, Z. Ruan, H. Wei, *et al.*, "First Demonstration of Differential-Drive Push-Pull Modulators on Thin-Film Lithium Niobate," Laser Photonics Rev. **19**(19), 2500018 (2025).
32. X. Zhu, Y. Hu, S. Lu, *et al.*, "Twenty-nine million intrinsic Q-factor monolithic microresonators on thin-film lithium niobate," Photonics Res. **12**(8), A63–A68 (2024).
33. H. Feng, T. Ge, Y. Hu, *et al.*, "On-chip optical vector analysis based on thin-film lithium niobate single-sideband modulators," Adv. Photonics **6**(06), 066006 (2024).
34. H. Feng, T. Ge, X. Guo, *et al.*, "Integrated lithium niobate microwave photonic processing engine," Nature **627**(8002), 80–87 (2024).
35. Y. Xie, H. Yan, Z. Wang, *et al.*, "Ultra-Wideband Tunable Thin-Film Lithium-Niobate-on-Insulator Microwave Photonic Filter," ACS Photonics **12**(3), 1689–1697 (2025).
36. H. Chi, X. Zou, and J. Yao, "Analytical models for phase-modulation-based microwave photonic systems with phase modulation to intensity modulation conversion using a dispersive device," J. Lightwave Technol. **27**(5), 511–521 (2009).
37. M. Liu, T. Zhang, B. Xu, *et al.*, "High-efficiency bident edge coupler based on thin film lithium niobate," Opt. Express **33**(7), 16338–16349 (2025).
38. G. Chen, K. Chen, Z. Yu, *et al.*, "Low-loss and broadband polarization-diversity edge coupler on a thinfilm lithium niobate platform," Opt. Lett. **48**(15), 4145–4148 (2023).
39. D. Jia, Q. Luo, C. Yang, *et al.*, "High-efficiency edge couplers enabled by vertically tapering on lithium-niobate photonic chips," Appl. Phys. Lett. **123**(26), 263502 (2023).
40. V. J. Urick Jr, J. D. Mckinney, and K. J. Williams, *Fundamentals of Microwave Photonics* (John Wiley & Sons, 2015), Chap. 2.
41. B. Masella and X. Zhang, "Linearized Optical Single-Sideband Mach–Zehnder Modulator for Radio-Over-Fiber Systems," IEEE Photonics Technol. Lett. **19**(24), 2024–2026 (2007).
42. J. Cardenas, P. A. Morton, J. B. Khurgin, *et al.*, "Linearized silicon modulator based on a ring-assisted Mach–Zehnder interferometer," Opt. Express **21**(19), 22549–22557 (2013).
43. S. Chen, G. Zhou, L. Zhou, *et al.*, "High-Linearity Fano Resonance Modulator Using a Microring-Assisted Mach–Zehnder Structure," J. Lightwave Technol. **38**(13), 3395–3403 (2020).
44. Q. Zhang, H. Yu, L. Wang, *et al.*, "Silicon dual-series Mach–Zehnder modulator with high linearity," Opt. Lett. **44**(23), 5655–5658 (2019).
45. X. Huang, Y. Liu, D. Tu, *et al.*, "Linearity-Enhanced Dual-Parallel Mach–Zehnder Modulators Based on a Thin-Film Lithium Niobate Platform," Photonics **9**(3), 197 (2022).
46. A. Tiwari, A. Velamuri, A. Goswami, *et al.*, "A Compact and High-Q value SiN Microring Resonator for Microwave Photonic Applications," in *2024 IEEE Silicon Photonics Conference (SiPhotonics)* (IEEE, 2024), pp. 1–2.
47. Y. Yao, Y. Zhao, J. Dong, *et al.*, "Silicon integrated frequency-tunable microwave photonic bandpass filter," IET Optoelectron. **17**(2-3), 70–76 (2023).
48. E. J. Norberg, R. S. Guzzon, J. S. Parker, *et al.*, "Programmable photonic microwave filters monolithically integrated in InP–InGaAsP," J. Lightwave Technol. **29**(11), 1611–1619 (2011).